Universität Ulm
Fakultät für Mathematik und Wirtschaftswissenschaften

ulm university universität
uulm

The Mammalian Circadian Clock: An Application for Numerical Optimal Control

Bachelorarbeit

in Mathematik

vorgelegt von
Alexandra Erbach
am 14. September 2012

Gutachter

Prof. Dr. Dirk Lebiedz

Acknowledgements. I would like to thank my advisor, Prof. Dr. Dirk Lebiedz, for making it possible for me to write my thesis in this field, and for his support and his patience during my work.

Moreover, I would like to thank Marcel Rehberg for answering many questions and editing my thesis.

Ulm, September 2012.

Contents

Chapter 1
Introduction

Countless complex natural processes have been the subject of research for natural scientists from diverse fields. However, the biological, chemical or physical methods are often limited and this is where mathematical modeling and simulation can lead to a greater understanding and clarify many problems.

Also the circadian clock which is investigated in this work can be counted to those complex biological systems which could not have been completely resolved by natural scientific methods.

In this thesis, we exploit a mathematical model of the mammalian circadian oscillator in order to investigate the possibility of shifting circadian rhythms in a desired way by specific light input. We proceed step by step and put great emphasize on the biological background knowledge as well as the underlying mathematical theory.

Numerous physiological and cellular processes underly circadian regulation. In chapter 2, the biological correlations which drive this governing by the circadian oscillator will be explained. In this introductory chapter we will also point out how the biological mode of function of the circadian clock enables the representation of the biological system by a system of ordinary differential equations.

In order to understand the general underlying process of the circadian clock, the negative feedback mechanism, in chapter 3 we will present the Goodwin Model, a very simplified model consisting of three differential equations. We will particularly focus on the model parameter which is mainly responsible for the generation of the sustained oscillations and investigate which requirements have to be complied with for their existence.

In chapter 4 we will present a more detailed and realistic clock model that takes an additional positive feedback loop into account and displays all the characteristic properties of the mammalian circadian clock. After the derivation of the model and its numerical solution, we are particularly interested in the impact of light input.

Chapter 5 contains the major component of this work. It shows how specific light influence can be used to shift the system to a desired phase. The theoretical background of optimal control is explained and then we apply the theory to the model of chapter 4.

In chapter 6, a conclusion and an outlook into possible future work is given.

Chapter 2

The mammalian circadian clock

The earth rotates around its own axis imposing a regular 24-hour pattern of light and darkness. Organisms as diverse as plants, insects and mammals have adapted to this daily pattern by developing biological rhythms. These are called circadian rhythms (lat. *circa diem*: approximately one day) and apply to many physiological processes such as renal and metabolic activity, hormone secretion, heart rate and blood pressure, body temperature and cellular processes which all fluctuate with a period close to 24 hours [8].

Four major features are characteristic for circadian rhythms:

- A circadian period of about 24 hours.
- The ability of entrainment to the external light-dark cycle.
- The persistence of the rhythms in the absence of external stimuli.
- The maintenance of the circadian periodicity over a range of temperatures (robustness).

A circadian clock is an oscillating biochemical mechanism that establishes a circadian rhythm. The master circadian clock in mammals that enables the link to the external light-dark cycle is located in the suprachiasmatic nucleus (SCN). The eyes contain several types of specialized light-sensitive cells which project the information about light and darkness to the SCN. The SCN integrates and forwards signals from the visual system and the periphery, coordinating circadian clocks in many organs and cells and synchronizing them with the external day/night cycle.

A lack of synchrony between the master clock in the brain and the external environment, called circadian misalignment, can lead to sleep disorders and lower productivity or even to long-term health problems such as diabetes, obesity, and cardiovascular disorders [26]. Circumstances and events which implicate irregular light/dark exposures, for example shift work or transcontinental flights, can contribute to circadian disruption [20].

Circadian rhythms are endogenous, that means that a period of approximately 24 hours is maintained even in the absence of external cues, as in constant darkness. The period of a circadian clock should generally be robust towards changes in the environment. Circadian rhythms display temperature compensation which allows the clock to maintain its periodicity despite changing reaction kinetics that influence all molecular processes in the cell [8].

2.1 Mechanism of the molecular oscillator

The molecular mechanisms that lead to the circadian oscillations are feedback loops in which the proteins which are encoded by the so-called 'clock genes' activate or inhibit their own production. The exact genes and proteins involved differ from species to species in mammals. We will take the circadian oscillator in mice as an example. Up to now, this is the mammal with the greatest amount of data available.

The core of the circadian oscillator can be considered a delayed negative feedback loop. Experiments in circadian systems of Neurospora, Drosophila and mammals as well as theoretical studies have shown the importance of a delayed negative feedback loop for the generation of oscillations [12].

The proteins BMAL1 and CLOCK act as transcription factors and activate the transcription of the period genes *Per1*, *Per2*, and *Per3* and the cryptochrome genes *Cry1* and *Cry2*. Consequently, there is an increase in the concentrations of *Per* and *Cry* mRNA and thereupon the levels of the PER and CRY proteins rise as well. A few hours after the peak of the mRNA concentration, those proteins accumulate in the nucleus where they bind to BMAL1 and CLOCK and deactivate the transcription factors. Hence, they inhibit their own transcription and the levels of *Per* and *Cry* mRNA decrease again, followed by the decrease of the corresponding protein concentrations. Now the transcription factors regain their active state and the whole process starts from the beginning, therefore inducing the typical oscillatory behavior.

The delay between transcription and nuclear accumulation which is essential in order to produce oscillations is a result of biological processes like post-translational modification, degradation, transport and complex formation [29].

In addition, there are positive feedback loops whose roles are much less understood. Interlocked feedback loops theoretically enable multiple inputs and outputs at different phases and it is assumed that positive feedback contributes to the robustness of the circadian clock [24].

PER2 promotes its own transcription by acting as a transcriptional activator for *Bmal1*. Whereas the concentration of CLOCK is fairly constant, the levels of *Bmal1* mRNA and protein display an oscillatory behavior. Another clock gene, *Rev-Erbα*, is involved in this feedback loop. REV-ERBα is a transcription factor that rhythmically represses the transcription of *Bmal1*. The feedback loops are interlaced: *Rev-Erbα* on the other hand is presumably activated by BMAL1 and inhibited by PER and CRY proteins [24]. A schematic view of the molecular mechanisms of the circadian oscillator is shown in Figure 2.1.

The number of known clock genes involved in various interlocked feedback loops is still increasing. This makes the biological circadian clock a very complex system that might not be completely understood for a long time.

2.2 Modeling the circadian clock

The circadian clock can be modeled as a nonlinear system of differential equations where the variables represent its molecular components and the parameters their properties. The interactions between the different components are represented by

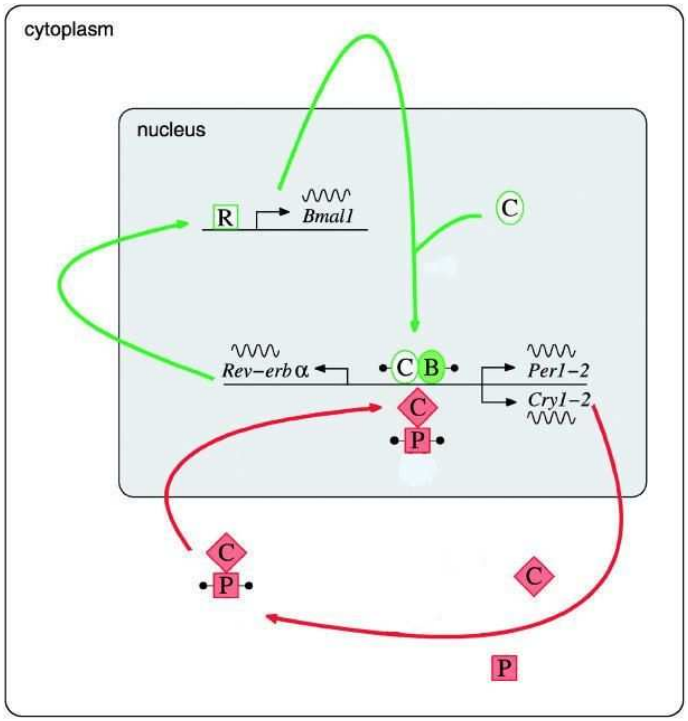

Fig. 2.1: Schematic view of the mammalian circadian core oscillator. The clock mechanism consists of interlaced positive (green) and negative (red) feedback loops. The heterodimer BMAL1/CLOCK (C, B, green ovals) promotes the transcription of *Per*, *Cry* and *Rev-erbα* genes. PER proteins (P, red square) are phosphorylated (•) and form a complex with CRY proteins (C, red diamond). In the nucleus, this complex acts as a transcriptional inhibitor of BMAL1/CLOCK, thus forming the negative feedback loop. In the positive feedback loop, the transcription of *Bmal1* is driven by PER/CRY, as this complex also inhibits REV-ERBα synthesis (R, green square), which in turn represses *Bmal1* transcription. Modified from [2].

the couplings between the equations. As the circadian clock is a biological system that has been studied extensively, many mathematical models have been proposed([13],[19],[10]). Depending on the number of variables and parameters involved, the complexity of the model and hence the extent to which it represents the molecular events of the actual biological system vary greatly. Smaller, more abstracted models may provide a more conceptual understanding.

The circadian clock is modeled as a limit cycle oscillator (LCO). In limit cycle oscillators, the periodic orbit is isolated and closed and its position and shape in the phase space is only dependent on the parameter values, not on initial conditions as long as those lie in the region of attraction of the periodic orbit. The stable limit cycle trajectory is asymptotically approached from any initial point that lies in the interior of this region of attraction. An essential property of limit cycle oscillations is the ability to return to the original oscillation after a disturbance in one or more state variables. This is a characteristic feature of the circadian clock oscillator, which is on one hand robust towards perturbations with respect to period and amplitude, but on the other hand entrainable to a specific phase by external stimuli [8].

This explains why LCOs are an intuitive choice for modeling the biological oscillators in the circadian clock mechanism. LCOs are always governed by nonlinear systems of ordinary differential equations [31].

Chapter 3
The Goodwin model

At first, we want to introduce the Goodwin model [13], which is one of the simplest models for circadian oscillators. It rather represents the general mechanism of a negative feedback repression than the complex mechanism of the circadian clock. It consists of no more than three differential equations with only one non-linear term and therefore enables an analytic approach.

3.1 Model set up

The system reads

$$\begin{aligned} \frac{dM}{dt} &= \frac{A_1}{A_2 + K_1 I^p} - aM, \\ \frac{dP}{dt} &= \beta M - bP, \\ \frac{dI}{dt} &= \gamma P - cI. \end{aligned} \tag{3.1}$$

The synthesis of a protein P is proportional to the amount of mRNA M. The post-translationally modified nuclear form of the protein is represented by I and acts as a transcription inhibitor. The production of the inhibitor I is proportional to the amount of P. I down-regulates the transcription of M. All three components M, P, and I degrade at rates proportional to their concentrations in the cell. The parameter K_1 describes the equilibrium constant of the first equation.

The Hill-coefficient p in the first equation generally describes the cooperativity of an end product repression. In biochemical reactions, the binding of a ligand to a macromolecule may be enhanced or inhibited if there are already other ligands bound to that macromolecule. The Hill-coefficient provides a way to quantify this effect, thereby indicating positive cooperativity if it is greater than one. In circadian models, Hill-coefficients are widely used even though they do most certainly not represent a cooperative effect in the classical sense. In our case, the Hill-coefficient models switch-like changes in the transcription rate as a response to small changes in the amount of the inhibitor I.

In the following, we want to analyze the effect of the value of p on the oscillatory behavior of the system. Sufficient amplification of the signal that is feeding back is essential for the appearance of oscillations. We will see that this can be attained by using a large Hill-coefficient.

In order to minimize the number of parameters involved, we non-dimensionalize the system (3.1) through a change of variables with $x = \frac{A_2}{A_1} M$, $y = \frac{A_2}{A_1 \beta} P$ and $z = \frac{A_2}{A_1 \beta \gamma} I$.

This yields

$$\begin{aligned} \dot{x} &= \frac{1}{1+Kz^p} - ax, \\ \dot{y} &= x - by, \\ \dot{z} &= y - cz, \end{aligned} \tag{3.2}$$

where $K = \frac{\beta^p \gamma^p {A_1}^p K_1}{{A_2}^{p+1}}$.
All parameters are assumed to be positive and we consider only the biologically relevant region where x, y and z are positive.

3.2 Stability and bifurcation analysis

The system can not be solved analytically, but we can use linearization for the stability analysis. The Jacobian matrix of system (3.2) is given by

$$J(x,y,z) = \begin{pmatrix} -a & 0 & \frac{-pKz^{p-1}}{(1+Kz^p)^2} \\ 1 & -b & 0 \\ 0 & 1 & -c \end{pmatrix} \tag{3.3}$$

and the characteristic equation is given by

$$(\lambda + a)(\lambda + b)(\lambda + c) + \frac{pKz^{p-1}}{(1+Kz^p)^2} = 0. \tag{3.4}$$

The stability of an equilibrium point (x^*, y^*, z^*) is determined by the eigenvalues of the Jacobian matrix evaluated at the corresponding equilibrium. By the Routh-Hurwitz criterion we know that an equilibrium point of a system of three differential equations with the characteristic equation $\lambda^3 + c_2\lambda^2 + c_1\lambda + c_0 = 0$ is asymptotically stable if c_2, c_1 and c_0 are positive and if additionally $D := c_2c_1 - c_0 > 0$.
In order to check whether these criteria are fulfilled, we need to evaluate the Jacobian matrix (3.3) at the steady state (x^*, y^*, z^*) and make some simplifications.
By inserting $\dot{x} = \dot{y} = \dot{z} = 0$ in the system (3.2), we obtain

$$y^* = cz^*, \tag{3.5}$$

$$x^* = by^* = bcz^*, \tag{3.6}$$

$$abcz^* = \frac{1}{1+Kz^{*p}}. \tag{3.7}$$

Hence we have $z^{*p} = \frac{1-abcz^*}{Kabcz^*}$ and inserting this in the last summand of equation (3.4) yields

$$\frac{pKz^{*p-1}}{(1+Kz^{*p})^2} = \frac{pKz^{*p}}{(1+Kz^{*p})^2 z^*} = pK \cdot \frac{1-abcz^*}{Kabcz^*z^*} \cdot (abcz^*)^2 = pabc \cdot (1-abcz^*). \tag{3.8}$$

In our case, we now have

$$\begin{aligned} c_2 &= a + b + c > 0, \\ c_1 &= ab + bc + ca > 0, \\ c_0 &= abc + pabc \cdot (1 - abcz^*) > 0. \end{aligned} \tag{3.9}$$

By using the inequality of Hardy, Littlewood and Polya [17]

$$\frac{1}{3}\left(x_1+x_2+x_3\right) \geq \left(\frac{1}{3}\left(x_1x_2+x_2x_3+x_3x_1\right)\right)^{\frac{1}{2}} \geq \left(x_1x_2x_3\right)^{\frac{1}{3}}, \tag{3.10}$$

which holds for all positive x_1, x_2 and x_3, we obtain

$$c_2c_1 \geq 3\left(\frac{1}{3}c_1\right)^{\frac{1}{2}} \cdot c_1 \geq 3c_1\left(abc\right)^{\frac{1}{3}} \geq 3 \cdot 3\left(abc\right)^{\frac{2}{3}}\left(abc\right)^{\frac{1}{3}} = 9abc \tag{3.11}$$

and therefore

$$\begin{aligned} D &= c_2c_1 - c_0 \\ &\geq 9abc - abc - pabc(1-abcz^*) \\ &= abc(8-p) + pa^2b^2c^2z^*. \end{aligned} \tag{3.12}$$

Now it is clear that D is always positive and hence the equilibrium is stable if $p \leq 8$. Only if the Hill-coefficient is greater than 8, an adequate choice of a, b, and c can make D negative and the steady state unstable. In this case, the steady state undergoes a Hopf bifurcation, a limit cycle is born and oscillations can be obtained.

We can show that for $p > 8$, it is always possible to make D negative and hence obtain oscillations. For if we set $a = b = c$ and define $\epsilon := abc$, the equations (3.11) and (3.12) become equalities and we then require

$$\epsilon z^* < 1 - \frac{8}{p} \tag{3.13}$$

for D to be negative. Because of (3.7), at the same time

$$\epsilon z^*(1 + Kz^{*p}) = 1 \tag{3.14}$$

holds. Now it follows from (3.14) that for $\epsilon \to 0$, we have $z^* \to \infty$ and therefore also

$$\epsilon z^* = \frac{1}{1+Kz^{*p}} \to 0, \tag{3.15}$$

so in this case (3.13) can always be satisfied by choosing ϵ small enough and hence sustained oscillations can be obtained [15].

Numerical simulations show that indeed oscillations do not occur if $p \leq 8$, that means that the cooperativity of feedback must generally be very high. For all calculations, we have set $K = 1$.

Figure 3.1 shows a bifurcation diagram with varying p and degradation rate constant a. The lines represent the boundary between parameter sets leading to oscillations and stable steady states. Oscillations are obtained to the right hand side of the lines. Choosing one of the other two constants b or c instead gives qualitatively the same results. If the constants are not nearly equal, but if one them is significantly larger than the other two, p_{min} increases dramatically and the region of the parameter space for which the system oscillates reduces [9]. For example, if $a = 0.3$, $b = 2$ and $c = 0.35$, then p_{min} is 22.

The calculation of the steady state which is necessary in order to start the numerical bifurcation analysis is done by using a damped Newton algorithm (see Appendix A.1).

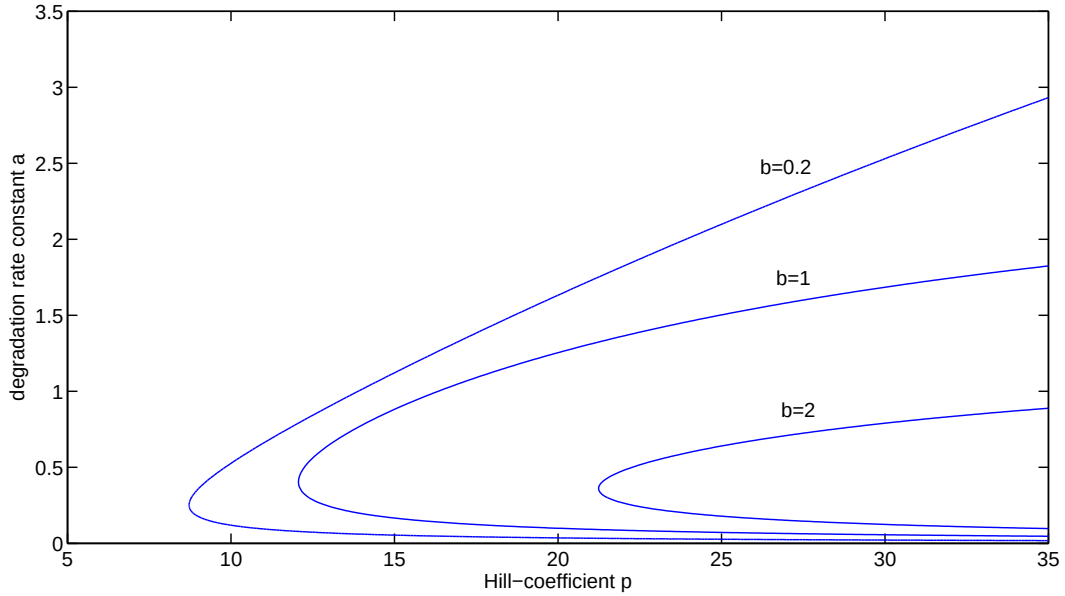

Fig. 3.1: Bifurcation diagram for $c = 0.35$ with varying p and a for different values of b. Oscillations are obtained to the right hand side of the lines.

It has been shown that replacing at least one of the linear degradation terms by a Michaelis-Menten term can lead to oscillations even with a Hill-coefficient $p \leq 8$ [2]. Michaelis-Menten kinetics describe the saturation of a reaction velocity and are used if a reaction rate is restricted to a maximum rate. This is a plausible assumption for degradation rates. Saturation of the degradation processes promotes oscillations and reduces the need for a very high cooperativity in the transcription process.

Already from that simple model it becomes obvious that the way in which the reaction kinetics are described has a great impact on the dynamic behavior of a model. Until more reliable data is available, we depend on making assumptions about how the circadian oscillations in the cell arise exactly.

Chapter 4

A mammalian clock model and the impact of light input

The delayed negative feedback loop can be considered the core of the circadian oscillator and is found throughout species. In this chapter we are going to introduce a more detailed model of the mammalian circadian clock that takes an additional positive feedback loop into account. As mentioned in chapter 2, in this feedback loop *Bmal1* activates its own transcription by increasing the amount of its transcriptional activator PER2. The system displays the essential properties of the circadian clock and shows an oscillatory behavior which is in good agreement with experimental data, but is still minimized with respect to the number of components and the kinetic complexity.

In section 4.3, we are particularly interested in the influence of light input on the model.

4.1 Model set up

Of the *Per* homologues, *Per3* seems to play a minor role in the core oscillator [8] and is not explicitly modeled. *Per1* is not modeled either, as its specific role within the positive or negative feedback is not fully understood. The absence of only *Per1* does not erase rhythmicity, but the absence of *Per2* leads to a continuous decay of the amplitude of the oscillations [10]. However, *Per1* could theoretically be included as it has been done for more detailed models. Moreover, as many features of the exact functional differences of *Per2*, *Cry1* and *Cry2* are not known yet and as they display similar properties, *Per2* and *Cry* mRNAS and proteins will be represented by the same variables, respectively, in order to keep the number of variables and parameters in the system low.

We take into account the transcriptional activation by BMAL1, but the constantly expressed CLOCK [21] can be treated as a fixed parameter. In the positive feedback loop, the transcription of *Rev-erbα* is down-regulated by the PER2/CRY proteins whereas REV-ERBα inhibits the transcription of *Bmal1*. Therefore, REV-ERBα is implicitly included in the model as we assume that the PER2/CRY complex promotes *Bmal1* transcription.

Phosphorylation of PER and CRY is not included in the model. We assume fast phosphorylation and rapid degradation of the monomeric PER2 and CRY proteins which implicates a quasi-steady state of those. The only post-translational modification present is an activation step for BMAL1.

With the assumptions set forth above, the model as it has been presented in [2] reads

$$\frac{dy_1}{dt} = \frac{v_{1b}(y_7 + c)}{k_{1b}\left(1 + \frac{{y_3}^p}{{k_{1i}}^p}\right) + (y_7 + c)} - k_{1d}y_1, \tag{4.1}$$

$$\frac{dy_2}{dt} = k_{2b}{y_1}^q - k_{2d}y_2 - k_{2t}y_2 + k_{3t}y_3, \tag{4.2}$$

$$\frac{dy_3}{dt} = k_{2t}y_2 - k_{3t}y_3 - k_{3d}y_3, \tag{4.3}$$

$$\frac{dy_4}{dt} = \frac{v_{4b}{y_3}^r}{{k_{4b}}^r + {y_3}^r} - k_{4d}y_4, \tag{4.4}$$

$$\frac{dy_5}{dt} = k_{5b}y_4 - k_{5d}y_5 - k_{5t}y_5 + k_{6t}y_6, \tag{4.5}$$

$$\frac{dy_6}{dt} = k_{5t}y_5 - k_{6t}y_6 - k_{6d}y_6 + k_{7a}y_7 - k_{6a}y_6, \tag{4.6}$$

$$\frac{dy_7}{dt} = k_{6a}y_6 - k_{7a}y_7 - k_{7d}y_7. \tag{4.7}$$

The variable y_1 represents the concentration of *Per2/Cry* mRNA. The concentration of cytoplasmatic PER2/CRY proteins is represented by y_2, and y_3 represents the concentration of the nuclear PER2/CRY complex that acts as the inhibitor of BMAL1. The concentration of *Bmal1* mRNA is represented by the variable y_4, the concentration of BMAL1 protein in the cytoplasm by y_5 and the one of nuclear BMAL1 protein by y_6. The variable y_7 describes the concentration of the transcriptionally active form of BMAL1 (BMAL1*) which can for example be interpreted as a phosphorylated form in a complex with CLOCK [11].

Figure 4.1 depicts the interactions between the model components. A description of the corresponding parameters is given in Table 4.1.

The transcription rates of *Per2/Cry*

$$f_{Per2/Cry} = \frac{v_{1b}(y_7 + c)}{k_{1b}\left(1 + \frac{{y_3}^p}{{k_{1i}}^p}\right) + (y_7 + c)} \tag{4.8}$$

and of *Bmal1*

$$f_{Bmal1} = \frac{v_{4b}{y_3}^r}{{k_{4t}}^r + {y_3}^r} \tag{4.9}$$

are described by Hill functions which represent the switch-like behavior in response to small changes of inhibitor concentration.

As mentioned before, many details of the molecular processes in the circadian oscillator are not known yet. The combined use of linear kinetics and high Hill-coefficients keeps the number of parameters in the system low and reduces the number of reaction steps that is necessary to obtain sustained oscillations.

Tab. 4.1: Parameters of the model including two feedback loops

Parameter	Description	Parameter Value
v_{1b}	Maximal rate of *Per2/Cry* transcription	9 nMh^{-1}
k_{1b}	Michaelis constant of *Per2/Cry* transcription	1 nM
k_{1i}	Inhibition constant of *Per2/Cry* transcription	0.56 nM
c	Concentration of constitutive activator	0.01 nM
p	Hill coefficent of inhibition of *Per2/Cry* transcription	8
k_{1d}	Degradation rate of *Per2/Cry* mRNA	0.12 h^{-1}
k_{2b}	Complex formation rate of PER2/CRY	0.3 $nM^{-1}h^{-1}$
q	Number of PER2/CRY complex forming subunits	2
k_{2d}	Degradation rate of the cytoplasmatic PER2/CRY	0.05 h^{-1}
k_{2t}	Nuclear import rate of the PER2/CRY complex	0.24 h^{-1}
k_{3t}	Nuclear export rate of the PER2/CRY complex	0.02 h^{-1}
k_{3d}	Degradation rate of the nuclear PER2/CRY complex	0.12 h^{-1}
v_{4b}	Maximal rate of *Bmal1* transcription	3.6 nMh^{-1}
k_{4b}	Michaelis constant of *Bmal1* transcription	2.16 nM
r	Hill coefficient of activation of *Bmal1* transcription	3
k_{4d}	Degradation rate of *Bmal1* mRNA	0.75 h^{-1}
k_{5b}	Translation rate of BMAL1	0.24 h^{-1}
k_{5d}	Degradation rate of cytoplasmatic BMAL1	0.06 h^{-1}
k_{5t}	Nuclear import rate of BMAL1	0.45 h^{-1}
k_{6t}	Nuclear export rate of BMAL1	0.12 h^{-1}
k_{6d}	Degradation rate of nuclear BMAL1	0.12 h^{-1}
k_{6a}	Activation rate of nuclear BMAL1	0.09 h^{-1}
k_{7a}	Deactivation rate of nuclear BMAL1*	0.003 h^{-1}
k_{7d}	Degradation rate of nuclear BMAL1*	0.09 h^{-1}

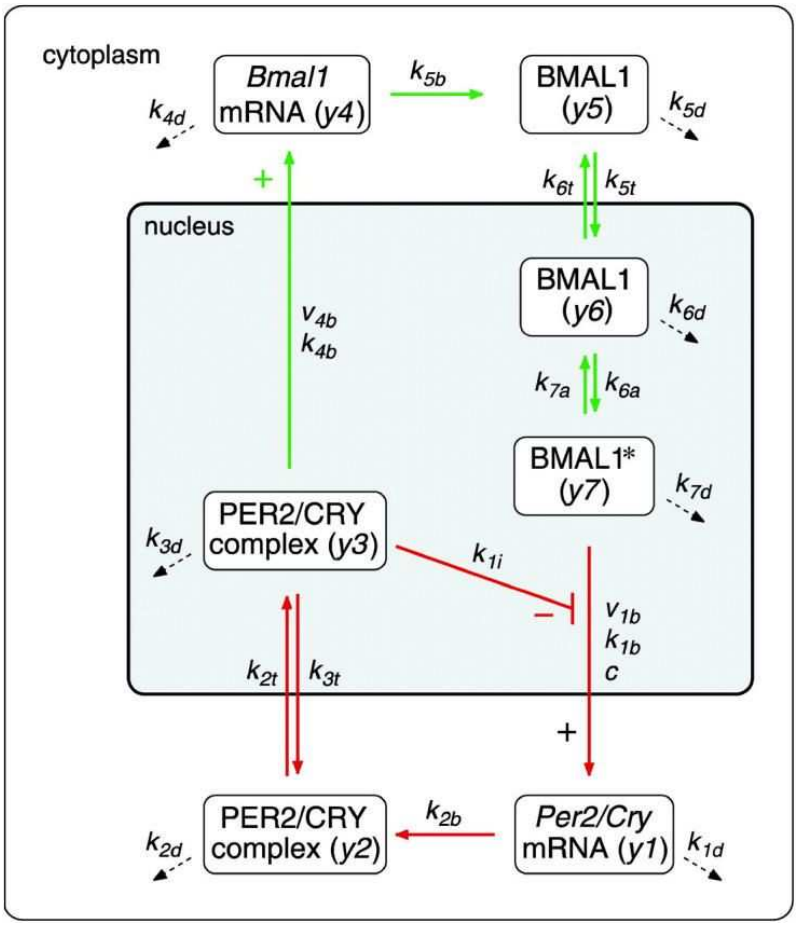

Fig. 4.1: Model of the circadian oscillator including a positive and a negative feedback loop. The activated BMAL* (y_7) acts as a transcription factor for *Per2* and *Cry* and increases the amount of *Per2/Cry* mRNA (y_1). The PER2 and CRY proteins form a complex (y_2) which is translocated into the nucleus. The nuclear PER2/CRY complex (y_3) binds to BMAL*, inhibiting *Per2/Cry* transcription (negative feedback loop) but at the same time promoting *Bmal1* transcription. The levels of *Bmal1* mRNA (y_4) and consequently of BMAL1 protein (y_5) rise. Eventually, nuclear BMAL1 (y_6) is activated (e.g. by phosphorylation and/or complex formation with CLOCK) and the active form BMAL1* (y_7) drives *Per2/Cry* transcription (positive feedback loop). The dotted arrows represent degradation. Taken from [2].

4.2 Numerical solution of the model

There exists a wide range of numerical methods to solve ordinary differential equations, for example various one-step and multi-step methods with both fixed and variable step sizes. The choice of the method is always problem-specific.

We chose the Dormand-Prince method used by the MATLAB ODE solver 'ode45' which is an explicit method based on a so-called Runge-Kutta formula. The ad-

vantage of explicit methods in comparison to implicit ones consists mainly in the reduced computational effort per integration step. We will briefly explain the concept of the Runge-Kutta algorithm.

Consider a general differential equation $y'(t) = f(t, y)$ and the resulting integral equation

$$y(t_{k+1}) - y(t_k) = \int_{t_k}^{t_{k+1}} f(t, y(t))dt. \tag{4.10}$$

We can approximate the integral by a general quadrature formula and obtain thereby the recursion formula of the Runge-Kutta method of s stages:

$$y_{k+1} = y_k + h \sum_{i=1}^{s} c_i k_i, \tag{4.11}$$

where $h := t_{k+1} - t_k$ denotes the step size and the k_i are computed in every iteration by the recursive formula

$$k_i = f(t_k + ha_i, y_k + \sum_{j=1}^{i-1} b_{ij} k_j), \quad i = 1, \ldots, s. \tag{4.12}$$

The number of function evaluations per step s and the coefficients a_i, c_i and b_{ij} are characteristic for the particular form of the Runge-Kutta method and can be arranged in a so-called Butcher array:

$$\begin{array}{c|cccc} a_1 & b_{11} & b_{12} & \cdots & b_{1s} \\ a_2 & b_{21} & b_{22} & \cdots & b_{2s} \\ \vdots & \vdots & \vdots & \ddots & \vdots \\ a_s & b_{s1} & b_{s2} & \cdots & b_{ss} \\ \hline & c_1 & c_2 & \cdots & c_s \end{array}$$

For all explicit Runge-Kutta methods, the Butcher array is a lower triangular matrix. The Dormand-Prince method calculates fourth- and fifth-order accurate solutions. The difference between these solutions is used as an approximation of the error of the fourth-order solution. This error estimate is essential for the adequate adaptation of the step size in every iteration [6].

The model was implemented and numerically solved in MATLAB. With the biologically plausible parameter values given in Table 4.1, the model shows sustained circadian oscillations with a period of 23.8 hours which is typical for mice, and correct phases between the oscillator components, as displayed in Figure 4.2.

4.3 Modeling light input

In the following, we are interested in the effect of light input on the system. In mammals, a short light pulse during subjective night induces the transcription of *Per1* and *Per2* in the SCN [22]. However, exact details about the correlation in mammals between the strength, duration and timing of an applied light pulse and

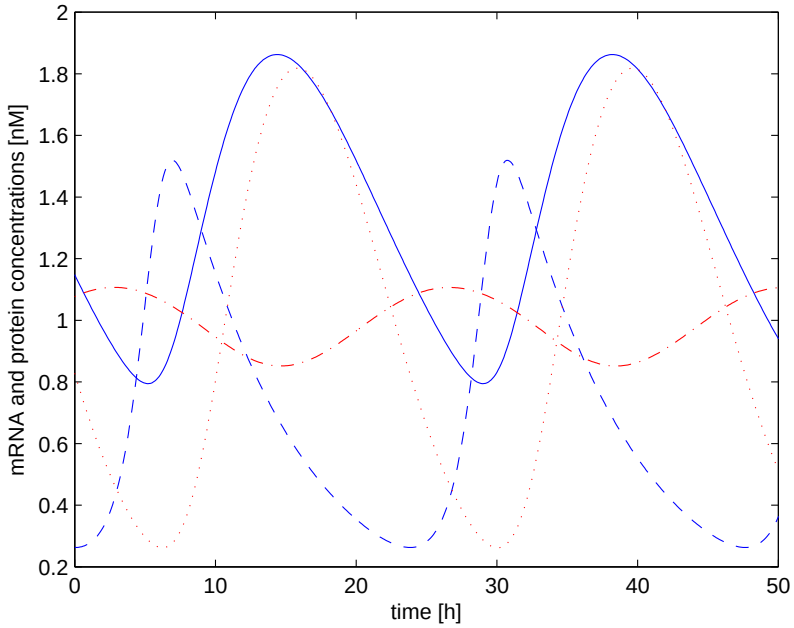

Fig. 4.2: Oscillations of the clock gene mRNAs and proteins with the parameter values given in Table 4.1. The dashed line represents *Per2/Cry* mRNA, the solid line nuclear PER2/CRY (y_3), the dotted line *Bmal1* mRNA (y_4) and the dash-dot line activated BMAL* (y_7). All model components oscillate with a period of 23.8 hours. Nuclear PER2/CRY protein shows a phase delay of 7.4 hours with respect to *Per2/Cry* mRNA, which is in agreement with experimental data.

the resulting differential increases in the transcription rates of the *Per* homologues are not known yet.

As only *Per2* is explicitly modeled, we neglect the functional differences between *Per1* and *Per2* with respect to light induction that were observed in experiments [32]. For simplicity we furthermore assume a continuous darkness scenario as basis for our numerical experiments.

4.3.1 Bifurcation analysis with respect to a light-sensitive parameter

In order to better understand the upcoming results, we will first investigate how the amplitude and the period of the oscillations depend on the multiplication of the *Per2/Cry* transcription rate $f_{Per2/Cry}$ (4.8) with a factor v that can be considered an extra parameter and represents a light-induced change of $f_{Per2/Cry}$.

Figure 4.3 shows the state variable y_1 representing the concentration of *Per2/Cry* mRNA as a function of v. The bifurcation diagram thus displays the dynamic behavior of the oscillatory system with respect to the light-controlled parameter v.

For low values of v, we have one up to three coexisting steady states. As v increases, the upper steady state undergoes a Hopf bifurcation and becomes unstable which

corresponds to the emergence of a stable limit cycle and the existence of sustained oscillations.

For a small range of parameter values, we can observe coexistence of a stable limit cycle and a stable steady state. This indicates that theoretically, light pulses could suppress the sustained circadian oscillations by moving the system into the basin of attraction of the stable equilibrium. However, $v = 1$ corresponds to a constant darkness scenario and we are therefore only interested in the behavior of the system for $v \geq 1$. For this parameter range, the system shows the desired stable oscillations with a relatively robust amplitude of the *Per2/Cry* mRNA oscillation.

The period seems to be robust towards changes in the value of the parameter v for $v \geq 1$ as well, as shown in Figure 4.4.

We can suspect that a finite light stimulus will always induce a deviation of the oscillating trajectory. However, in accordance with what we know about limit cycle oscillations, it will asymptotically return to the stable limit cycle. The system thereby undergoes a phase shift and the magnitude of the phase shift depends on the strength and timing of the stimulus.

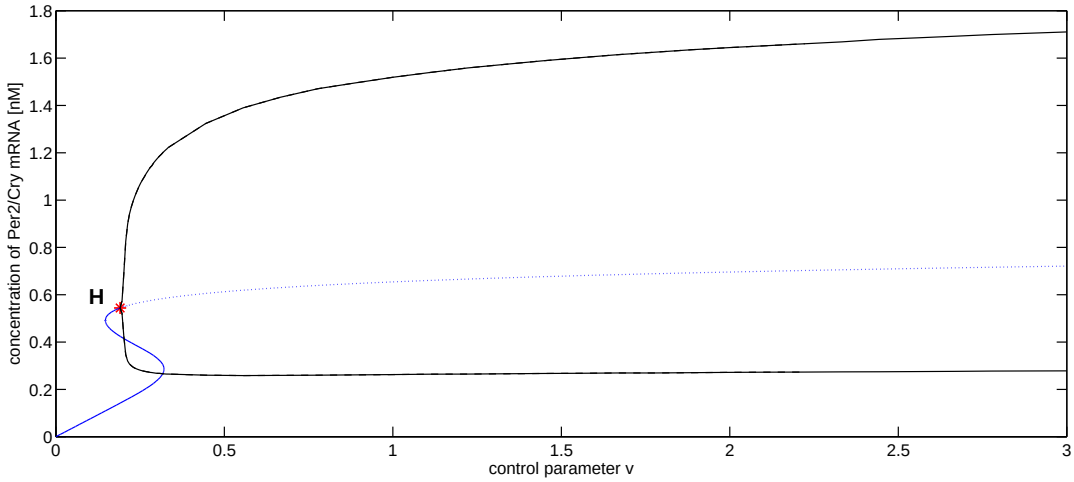

Fig. 4.3: Bifurcation diagram with respect to the light-sensitive parameter v. 'H' denotes a Hopf bifurcation. The solid black lines show maximum and minimum of the oscillation and represent the stable limit cycle. The dotted line indicates the unstable steady state. For $v = 1$, *Per2/Cry* mRNA concentration oscillates between 0.3 and 1.5 nM. For greater values of v, the amplitude of the oscillation increases only slightly.

4.3.2 Simulation of light pulses

We can represent light pulses by multiplying equation 4.1 with a piecewise constant function $v(t)$ and thus describe the temporary alteration of the rate of *Per2/Cry* transcription. A light pulse is simulated by a switch of $v(t)$ from 1 to a constant value $v_c > 1$. We somewhat arbitrarily assume that for our model, a short light pulse leads to a two hour period of a higher rate of *Per2/Cry* expression.

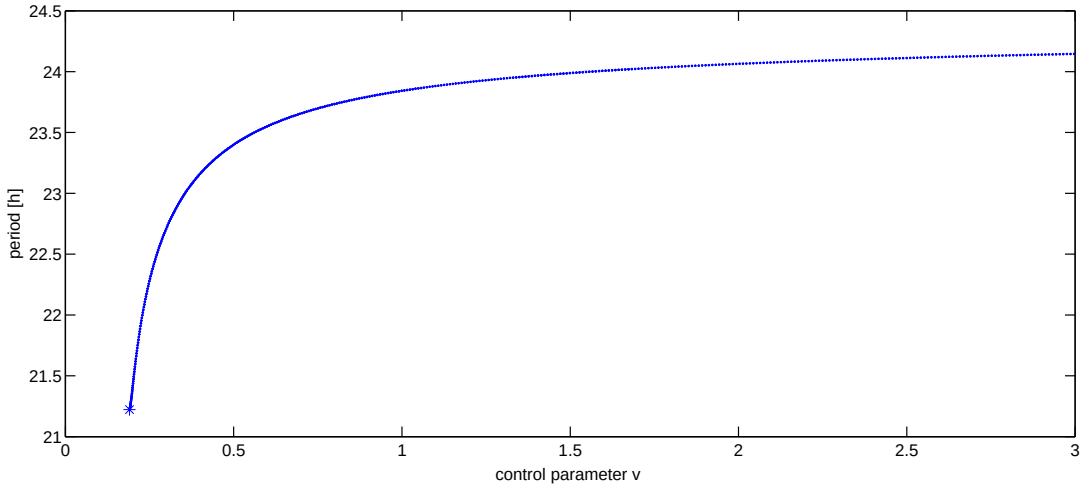

Fig. 4.4: Bifurcation diagram with respect to the light-sensitive parameter v. The period of the oscillation is sensitive toward parameter changes for low values of v, but becomes more robust for $v \geq 1$. For the default value $v = 1$, the system oscillates with a period of 23.8 hours as expected.

Equation 4.1 then reads

$$\frac{dy_1}{dt} = v(t) \cdot \frac{v_{1b}(y_7 + c)}{k_{1b}\left(1 + \frac{{y_3}^p}{{k_{1i}}^p}\right) + (y_7 + c)} - k_{1d} y_1, \tag{4.13}$$

where

$$v(t) = \begin{cases} v_c & \text{if } t \in [t_0, t_0 + 2] \\ 1 & \text{else} \end{cases} \tag{4.14}$$

The oscillation under free-running conditions is divided into 24 circadian hours and the phases range from CT (circadian time) 0 to CT 24, CT 0 being associated with subjective dusk and CT 12 with subjective dawn as introduced in [16]. In the SCN, the beginning of the rise of *Per* and *Cry* mRNA coincides with the beginning of subjective day [7]. Therefore, the minimum of *Per2*/*Cry* mRNA is set to be the time reference CT = 12.

The point $t_0 \in [0, 24]$ determines the phase at which the light pulse is received.

Circadian rhythms can be shifted by light pulses. Phase shifts are an essential property of periodic functions. The following definition establishes a mathematical relation between a time-shifted curve and an arbitrary reference curve.

Definition 4.3.1

Let $x(t) : \mathbb{R} \to \mathbb{R}^n$ be a periodic function with period τ, i.e. $x(t) = x(t+\tau)$ holds for all $t \in \mathbb{R}$. If we define a reference function $x_r(t)$ to have phase zero, we can define a time-shifted version

$$x_\phi(t) := x_r(t + \phi)$$

of x_r, where $\phi \in \left(-\frac{\tau}{2}, \frac{\tau}{2}\right]$. The time shift ϕ is called the phase of x_ϕ with respect to x_r.

The free-running period of our model oscillator is $\tau = 23.8h$. A phase response curve (PRC) represents the phase shift ϕ of an oscillation induced by a perturbation as a function of the time t_0 at which it is received. In order to obtain the PRC, we simulate light pulses for $t_0 \in \{0, 0.1, 0.2, \ldots, 23.9, 24\}$ and calculate the phase shift in *Per/Cry* oscillation after 7 days. As stated before, the curve where the minimum of *Per2/Cry* mRNA occurs at CT = 12 is said to be in zero phase, i.e. this is $x_r(t)$. The result of the numerical calculations is shown in Figure 4.5 for two different light input strengths.

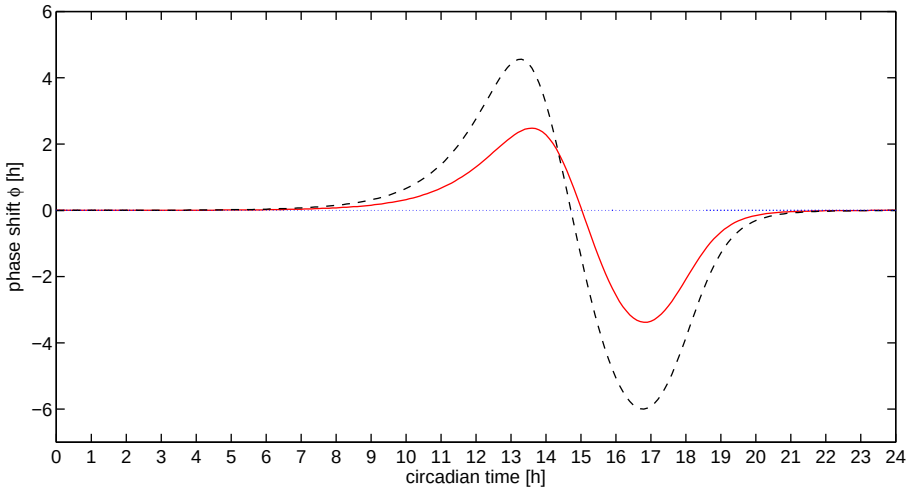

Fig. 4.5: Phase response curve of the model oscillator for light stimuli that are assumed to lead to a 2-hour period of a higher rate of *Per2/Cry* expression. The solid line shows the PRC for $v_c = 1.5$, the dashed line shows the PRC for $v_c = 2.5$. The dotted line indicates no light input.

Chapter 5
Phase tracking of circadian rhythm by numerical optimal control

As already mentioned in chapter 2, disorders of the circadian oscillator affect sleep and waking times and thus have an influence on sleep duration and quality. Misalignment between the internal circadian clock and the external light-dark cycle can even lead to serious health problems [25]. This knowledge motivates the study of control problems dedicated to manipulate circadian rhythms in a specific way. Mathematical models can thereby be exploited for analyzing potential control schemes.

In this thesis, we investigate how the phase of the circadian system can be brought into a desired state. The problem of phase-shifted circadian rhythms comes for example with circadian rhythm sleep disorders such as the delayed sleep-phase syndrome (DSPS) characterized by a significantly delayed timing of sleep onset and offset and a period of peak alertness in the middle of the night [4]. But also circumstantial disorders such as jet lag and the so-called shift work sleep disorder are related to a phase shift of the circadian rhythm. Besides administering hormones such as melatonin, bright light therapy has been shown to be a useful way of treatment [27].

Our aim in this chapter is to specifically influence the behavior of the system by time-varying external control stimuli, i.e. light pulses.

As stated in chapter 4, it has been shown that light input during subjective night enhances the transcription rates of the *Per* genes. In our model, we simulate light pulses by multiplication of the *Per2/Cry* transcription rate $f_{Per2/Cry}$ (Eq. 4.8) with a control function $u(t) \in [1, u_{max}]$, as introduced in [28].

Strictly speaking, we are interested in phase-shifting the system and synchronizing it with a defined reference trajectory. In order to do so, we need to identify the optimal strength and timing of the light-induced changes for *Per2/Cry* transcription that result in the desired phase shift.

Before we are going to solve our specific problem, we will give some explanation about the mathematical background.

5.1 Optimal control

Generally speaking, optimal control deals with the problem of finding an input for a given dynamical system such that a certain optimality criterion is minimized or

maximized. An optimal control problem always involves an objective function that is a function of state and control variables and returns a scalar value.

Our optimization problem consists of minimizing the deviation of the controlled state trajectory $x(t)$ from a reference trajectory $x_r(t)$ over a given time horizon T. The reference trajectory is obtained by integration of the system with initial values that we define to be related to zero phase condition, and constant control $u(t) \equiv 1$.

Our optimal control problem then reads

$$\min_{x,u} \int_0^T \|x(t) - x_r(t)\|_2^2 \, dt, \tag{5.1}$$

$$\text{subject to:} \tag{5.2}$$

$$\dot{x}(t) = f(x(t), u(t), p), \ t \in [0, T], \tag{5.3}$$

$$x(0) = x_0, \tag{5.4}$$

$$u(t) \in [1, u_{max}], \tag{5.5}$$

where f represents the system of differential equations of the model oscillator (Eqs. 4.1-4.7), p is the corresponding parameter vector containing all model parameters, $u(t) \in [1, u_{max}] \subset \mathbb{R}^+$ denotes the control function and $\|\cdot\|_2$ indicates the euclidean norm.

The mathematical theory in this section is taken from [5] and [1]. In the following, all parameter values will be fixed to the values given in Table 3.1.

In order to be able to obtain a numerical solution, we need to transform the infinite-dimensional control problem into a finite-dimensional nonlinear programming problem (NLP). This is possible by discretizing the control function as well as the differential equation.

For the discretization of the control function $u(t)$, the time interval $[0, T]$ is divided into N subintervals. We thus introduce a time grid of N+1 nodes:

$$0 = t_0 \leq t_1 \leq \cdots \leq t_N = T. \tag{5.6}$$

The time grid can be equidistant, but also subintervals with different length are possible. To improve the accuracy of the solution, we can increase N which consequently also increases the computational effort.

Piecewise constant functions $u_i(t) = q_i$ are used to represent $u(t)$ for $t \in [t_i, t_{i+1}]$ $(i = 0, \ldots, N-1)$. With N control parameters $q = (q_0, \ldots, q_{N-1})$ we obtain an approximation $\widehat{u}$ of $u(t)$ on the grid (5.6) by

$$\widehat{u}(t) = q_i \ \text{ for } \ t \in [t_i, t_{i+1}], \quad i = 0, \ldots, N-1. \tag{5.7}$$

Several methods are present in current literature for discretizing the ODE and solving the optimal control problem, such as single shooting, multiple shooting or the collocation method. We will present the sequential approach of direct single shooting and the multiple shooting method with simultaneous simulation and optimization and later apply both methods to our optimal control problem.

5.1.1 Direct single shooting

In this method, an adaptive numerical integration solver (e.g. ode45) is used to solve (5.3) on each interval given by the grid (5.6) and obtain the state as a function

$x(t;q)$ of the N control parameters $q = (q_0, \ldots, q_{N-1})$. By the discretization of the control function and the numerical ODE solution, we get the NLP

$$\begin{aligned} &\min_q \int_0^T \|x(t;q) - x_r(t)\|_2^2 \, dt, \\ &\text{subject to:} \\ &q_i \in [1, u_{max}], \ i = 0, \ldots, N-1. \end{aligned} \tag{5.8}$$

This NLP can now be solved with a finite dimensional optimization approach such as sequential quadratic programming (SQP) which we will introduce in the next section. A continuous trajectory is computed as a feasible ODE solution in every iteration of the optimization process. Figure 5.1 illustrates the general concept of direct single shooting.

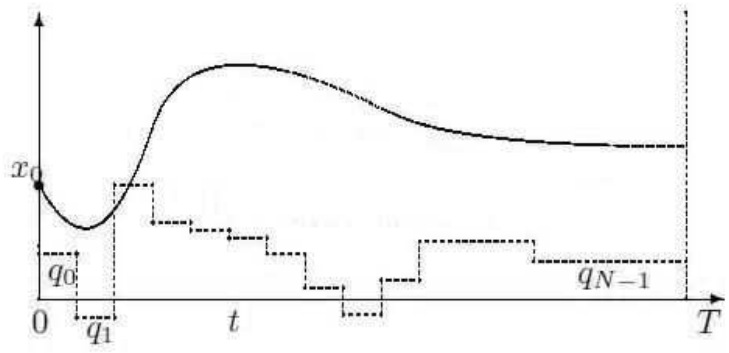

Fig. 5.1: Illustration of direct single shooting. Controls are discretized and the computed state trajectory is continuous. Taken from [5].

5.1.2 Direct multiple shooting

In contrast to the sequential approach of single shooting, the multiple shooting method proposed by Bock [3] solves the differential equation and the optimization problem at the same time.

On the grid (5.6), artificial node values $s = (s_0, \ldots, s_N)$ are established. Then, trajectory pieces $x_i(t; s_i, q_i)$ are obtained by numerically solving the differential equation on each of the multiple shooting intervals $[t_i, t_{i+1}]$, whereupon the node values s_i serve as initial values:

$$\begin{aligned} \dot{x}_i(t; s_i, q_i) &= f(x_i(t; s_i, q_i), q_i), \quad t \in [t_i, t_{i+1}], \\ x_i(t_i; s_i, q_i) &= s_i. \end{aligned}$$

Continuity of the state trajectory is ensured by including nonlinear equality constraints into the NLP. More precisely, we get a continuous solution over $[0, T]$ by matching the initial conditions s_{i+1} at t_{i+1} with the final values obtained from solving the ODE over the previous subinterval $[t_i, t_{i+1}]$. The initial values s_i are treated as optimization variables and are adjusted in every iteration of the optimization

process. The NLP now reads

$$\begin{aligned} &\min_{q,s} \int_0^T \|x(t;q,s) - x_r(t)\|_2^2 \, dt, \\ &\text{subject to:} \\ &q_i \in [1, u_{max}], \ i = 0, \ldots, N-1, \\ &s_{i+1} = x_i(t_{i+1}; s_i, q_i), \ i = 0, \ldots, N-1, \\ &s_0 = x_0. \end{aligned} \tag{5.9}$$

The general concept of direct multiple shooting is sketched in Figure 5.2.

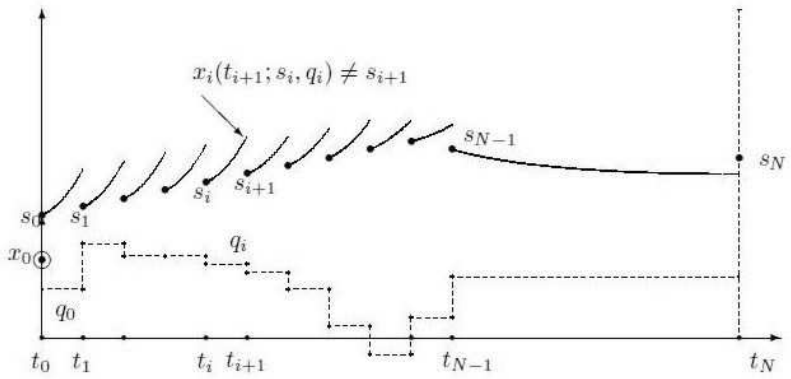

Fig. 5.2: Illustration of direct multiple shooting. Again, controls are discretized but matching conditions are violated at that time and the computed state trajectory is not yet continuous. Taken from [5].

If we summarize all variables in one vector $\omega = (q_0, s_0, q_1, s_1, \ldots, q_{N-1}, s_{N-1}, s_N)$, combine all equality constraints and continuity conditions in a function $H(\omega)$ and all inequality constraints in a function $G(\omega)$, we obtain the structured NLP

$$\begin{aligned} &\min_{\omega} F(\omega), \\ &\text{subject to:} \\ &G(\omega) \leq 0, \\ &H(\omega) = 0. \end{aligned} \tag{5.10}$$

Again, (5.10) can be solved with the standard SQP algorithm. Thereby, the continuity conditions do not necessarily have to be satisfied during the iterations of the optimization process.

As the number of degrees of freedom of the optimal control problem increases significantly compared to single shooting, the multiple shooting method does not necessarily converge faster. Its great advantage consists of its improved numerical stability and reduced non-linearity.

5.2 Sequential quadratic programming (SQP)

For the implementation in MATLAB, we use the solver *fmincon* with an active-set strategy. In the following, we will give some mathematical background on nonlinear constrained optimization and briefly explain how the algorithm works. Definitions and theorems in this section are taken from [18].

Consider the general constrained nonlinear optimization problem

$$\begin{aligned} &\text{minimize } f(x),\ x \in \mathbb{R}^n, \\ &\text{subject to:} \\ &g_i(x) \leq 0,\ i = 1, \cdots, m, \\ &h_j(x) = 0,\ j = 1, \cdots, p. \end{aligned} \tag{5.11}$$

We thus want to minimize the objective function f while maintaining all the inequality constraints g_i and all the equality constraints h_j. The functions f, g and h are assumed to be continuously differentiable on $\mathbb{R}^n$.

Definition 5.2.1 (Feasibility)
*The **feasible set** of (5.11) is defined by*

$$X := \{x \in \mathbb{R}^n : g_i(x) \leq 0 \text{ for all } i = 1, \dots m, \quad h_j(x) = 0 \text{ for all } j = 1, \dots p\}$$

*and every point $x \in X$ is called **feasible**.*

The aim is now to transform the problem (5.11) into an easier subproblem that can be solved and used as a basis for an iterative numerical process.

Definition 5.2.2 (The Lagrangian function)
*The **Lagrangian function** $\mathscr{L}$ is defined by*

$$\begin{aligned} \mathscr{L}(x, \mu, \lambda) &:= f(x) + \sum_{i=1}^{m} \mu_i g_i(x) + \sum_{j=1}^{p} \lambda_j h_j(x), \\ &= f(x) + \mu^T g(x) + \lambda^T h(x) \end{aligned}$$

*with the so-called **Lagrange multipliers** $\mu \in \mathbb{R}^m$ and $\lambda \in \mathbb{R}^p$.*

Definition 5.2.3 (The Karush-Kuhn-Tucker (KKT) equations)
Referring to the problem (5.11), the KKT-equations can be stated as

$$\begin{aligned} \mathscr{L}_x(x, \mu, \lambda) &= 0 \\ h_j(x) &= 0 \quad , j = 1, \cdots p \\ \mu_i &\geq 0, \quad i = 1, \cdots m \\ g_i(x) &\leq 0, \quad i = 1, \cdots m \\ \mu_i g_i(x) &= 0, \quad i = 1, \cdots m \end{aligned} \tag{5.12}$$

In the first equation we have the gradient of the Lagrangian function $\mathscr{L}$ with respect to x: $\mathscr{L}_x(x, \mu, \lambda) = \nabla f(x) + \sum_{i=1}^{m} \mu_i \nabla g_i(x) + \sum_{j=1}^{p} \lambda_j \nabla h_j(x)$.

A point (x^*, μ^*, λ^*) that satisfies the conditions (5.12) is called a **KKT-point** of the optimization problem (5.11) with the corresponding Lagrange multipliers $\mu^* = ({\mu_1}^*, \dots {\mu_m}^*)$ and $\lambda^* = ({\lambda_1}^*, \dots, {\lambda_p}^*)$.

Definition 5.2.4 (Active Set)
*Referring to problem (5.11), consider a point x^* that satisfies all equality and inequality constraints. Then a constraint $g_i(x^*) \leq 0$ is called active at x^* if $g_i(x^*) = 0$. The **active set** $\mathscr{A}(x^*)$ is made up of the indexes of those constraints that are active at x^*.*

The idea of an active-set strategy is to get rid of the inequality constraints as we will explain later in more detail.

Definition 5.2.5 (Linear independence constraint qualification (LICQ))
A point $x^* \in X$ satisfies the linear independence constraint qualification if the gradients

$$\{\nabla h_j(x^*)\}_{j=1,\dots,p} \cup \{\nabla g_i(x^*)\}_{i \in \mathscr{A}(x^*)}$$

are linearly independent.

If a point x^* is a local minimum of (5.11) that satisfies the LICQ, then there exist unique Lagrangian multipliers λ^* and μ^* such that (x^*, μ^*, λ^*) is a KKT-point of (5.11).
The KKT-equations are first order necessary optimality conditions for a constrained nonlinear optimization problem and transform the problem into a nonlinear system of equalities and inequalities whose solution can be used as a basis to the programming algorithm.
If we consider the problem

$$\begin{aligned} &\min_x f(x), \\ &\text{subject to:} \\ &h(x) = 0, \end{aligned} \tag{5.13}$$

then the KKT-equations can be written as

$$\begin{pmatrix} 0 \\ 0 \end{pmatrix} = \phi(x, \lambda) := \begin{pmatrix} \mathscr{L}_x(x, \lambda) \\ h(x) \end{pmatrix}, \tag{5.14}$$

where $\mathscr{L}_x$ denotes the gradient with respect to x of the Lagrangian function $\mathscr{L}(x, \mu, \lambda) = f(x) + \sum_{j=1}^{p} \lambda_j h_j(x)$.
This gives us a nonlinear system with $(n+p)$ variables. Equation 5.14 can be solved by using the standard Newton method which obtains the increment $(\Delta x_k, \Delta \lambda_k)$ as solution of the equation

$$J_\phi(x_k, \lambda_k) \begin{pmatrix} \Delta x \\ \Delta \lambda \end{pmatrix} = -\phi(x_k, \lambda_k), \tag{5.15}$$

where $J_\phi = \begin{pmatrix} \nabla^2_{xx}\mathscr{L} & \nabla_x h \\ \nabla_x h^T & 0 \end{pmatrix}$ denotes the Jacobian matrix of ϕ.

The new iterate is obtained by $(x_{k+1}, \lambda_{k+1}) = (x_k + \Delta x_k, \lambda_k + \Delta\lambda_k)$.

If we define $H_k := \nabla^2_{xx}\mathscr{L}(x_k, \lambda_k)$, we can rewrite the system (5.15) as

$$\begin{aligned} H_k\Delta x_k + \nabla h(x_k)\Delta\lambda_k &= -\nabla_x\mathscr{L}(x_k, \lambda_k), \\ \nabla h(x_k)^T\Delta x_k &= -h(x_k). \end{aligned} \tag{5.16}$$

Now we can see that (5.16) and therefore also (5.15) is equivalent to

$$\begin{aligned} H_k\Delta x_k + \nabla h(x_k)\widetilde{\lambda} &= -\nabla f(x_k), \\ \nabla h(x_k)^T\Delta x_k &= -h(x_k), \end{aligned} \tag{5.17}$$

with $\widetilde{\lambda} := \lambda_k + \Delta\lambda_k$.

These are exactly the KKT-equations of the system

$$\begin{aligned} &\min_{\Delta x_k} \nabla f(x_k)^T\Delta x_k + \frac{1}{2}\Delta x_k^T H_k \Delta x_k, \\ &\text{subject to:} \\ &h(x_k) + \nabla h(x_k)^T\Delta x_k = 0, \end{aligned} \tag{5.18}$$

which now yields the idea to formulate and solve a **quadratic programming (QP) subproblem** for our original problem (5.11) of the form:

$$\begin{aligned} &\min_{d\in\mathbb{R}^n} \nabla f(x_k)^T d + \frac{1}{2} d^T \widetilde{H}_k d, \\ &\text{subject to:} \\ &g(x_k) + \nabla g(x_k)^T d \le 0, \\ &h(x_k) + \nabla h(x_k)^T d = 0. \end{aligned} \tag{5.19}$$

The solution d_k of (5.19) is then used to obtain a new iterate $x_{k+1} = x_k + \alpha_k d_k$ of the desired solution x of (5.11). The step length α_k is determined by an appropriate line search procedure. The matrix $\widetilde{H}_k$ is a positive definite quasi-Newton approximation of the Hessian of the Lagrangian function, $\nabla^2_{xx}\mathscr{L}(x_k, \mu_k, \lambda_k)$, and is updated in every iteration.

As a QP has to be solved in every main iteration, the method is called **Sequential Quadratic Programming (SQP)**.

The solution of an equality constrained QP can directly be obtained as the solution of a linear system, as those are strict convex NLP where the KKT-equations are both necessary and sufficient for a global solution point.

In order to deal with the inequalities, an active-set strategy is used. In the algorithm, an active set $\mathscr{A}_k$ is maintained that is an estimate of the active constraints at the solution point. $\mathscr{A}_k$ is updated in every iteration k of the QP method and we thereby obtain a sequence of equality constrained QP that can be solved.

5.3 Phase tracking of circadian rhythm: Implementation

The circadian rhythm can be successfully tracked by continuously adjustable light stimuli. We want to identify strength and timing of the light-switching-induced changes in the *Per2/Cry* mRNA transcription rate that reduce the phase difference to the desired reference trajectory in minimal time. Our aim is to find a controller which is able to recover a phase difference of up to 12 hours. We will apply both single and multiple shooting to our problem.

5.3.1 Numerical implementation with single shooting

We have already introduced and explained the formulation of our optimal control problem. For the numerical implementation, we set the final time $T = 72$ and $u_{max} = 3$. If we assume that a light pulse leads to a two hour period of enhanced *Per2/Cry* transcription and use the single shooting method, the NLP (5.8) reads

$$\begin{aligned} &\min_{q} \int_0^{72} \|x(t;q) - x_r(t)\|_2^2 \, dt, \\ &\text{subject to:} \\ &q_i \in [1,3]\,,\ i = 0, \dots 35. \end{aligned} \tag{5.20}$$

As before we define for a curve to be in zero phase if the minimum of *Per2/Cry* mRNA occurs at CT 12 which corresponds to the beginning of subjective day. Integration of the system with initial values that correspond to this zero phase condition gives us the reference trajectory $x_r(t)$.

The controller is able to recover a phase difference of 12 hours within approximately 60 hours with high accuracy (Fig. 5.3). Although only the results of the concentration of *Per2/Cry* mRNA are shown, all seven variable concentrations were tracked to the reference trajectory. The circadian rhythm could successfully be restored. Figure 5.4 shows the controls obtained by the numerical optimization. The corresponding MATLAB-file can be found in Appendix A.2.

5.3.2 Numerical implementation with multiple shooting

We can also solve the optimal control problem using the multiple shooting method. Again, we set the final time $T = 72$ and $u_{max} = 3$. In order to decrease the number of degrees of freedom, we now assume that a light pulse leads to a three hour instead of a two hour period of a higher rate of *Per2/Cry* transcription.
The NLP then reads

$$\begin{aligned} &\min_{q,s} \int_0^{72} \|x(t;q,s) - x_r(t)\|_2^2 \, dt, \\ &\text{subject to:} \\ &q_i \in [1,3]\,,\ i = 0, \dots 23, \\ &s_{i+1} = x_i(t_{i+1}; s_i, q_i),\ i = 0, \dots 23, \\ &s_0 = x_0. \end{aligned} \tag{5.21}$$

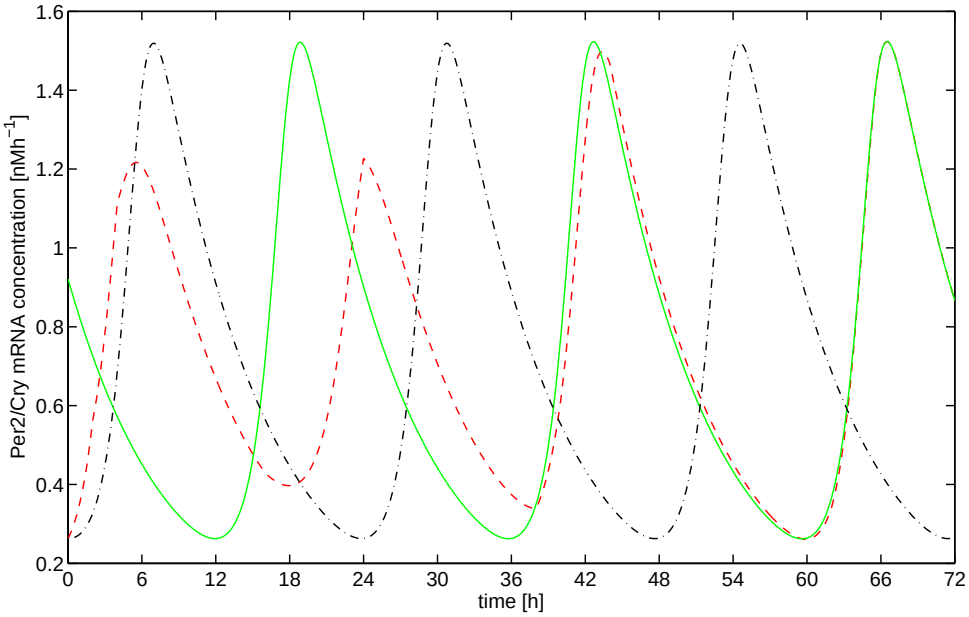

Fig. 5.3: Optimal control of circadian rhythm tracking of a 12-hour phase difference by light stimuli with single shooting. The solid curve represents the reference trajectory, the dashed curve shows the controlled system state trajectory (*Per2/Cry* mRNA concentration) and the dash-dot curve represents the uncontrolled system state trajectory (*Per2/Cry* mRNA concentration).

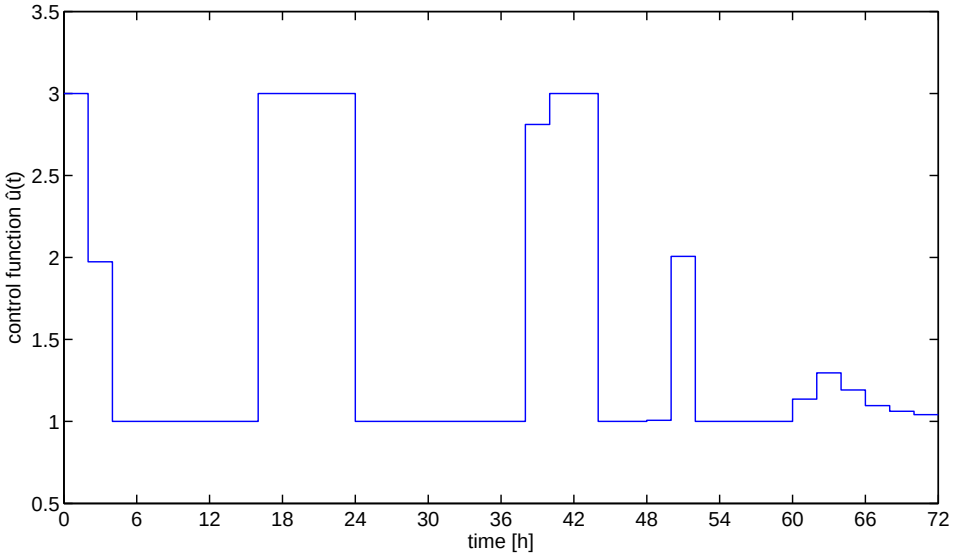

Fig. 5.4: Controls obtained by the numerical optimization with single shooting for a 12-hour phase shift. Values of the control function $\widehat{u}(t)$ have to be in the interval $[1, 3]$.

As shown in Figure 5.5, the results are very similar and again, the circadian rhythm could successfully be restored. Figure 5.6 shows the controls obtained by the numerical optimization using the multiple shooting algorithm. For the MATLAB-file, see Appendix A.3.

As the size of the optimization problem has been significantly increased and as a lot more function evaluations are necessary, it takes longer until convergence is achieved. The efficiency of the algorithm could be improved by using another method for the calculation of the sensitivities

$$\frac{\partial x(t;q,s)}{\partial q} \quad \text{and} \quad \frac{\partial x(t;q,s)}{\partial s}$$

of the numerical ODE solution $x(t;q,s)$ with respect to the controls q and the multiple shooting node values s, respectively. The default setting causes *fmincon* to estimate the derivatives using finite differences which is relatively expensive. An alternative is for example the technique of automatic differentiation (AD) [14] which is highly accurate and has been successfully used for optimal control problems. Also the gradients of the nonlinear constraints could be computed manually and then passed to the optimization solver in order to avoid the estimate of the gradients using finite differences. However, the numerical efficiency of the implementation shall not be of particular interest in this work.

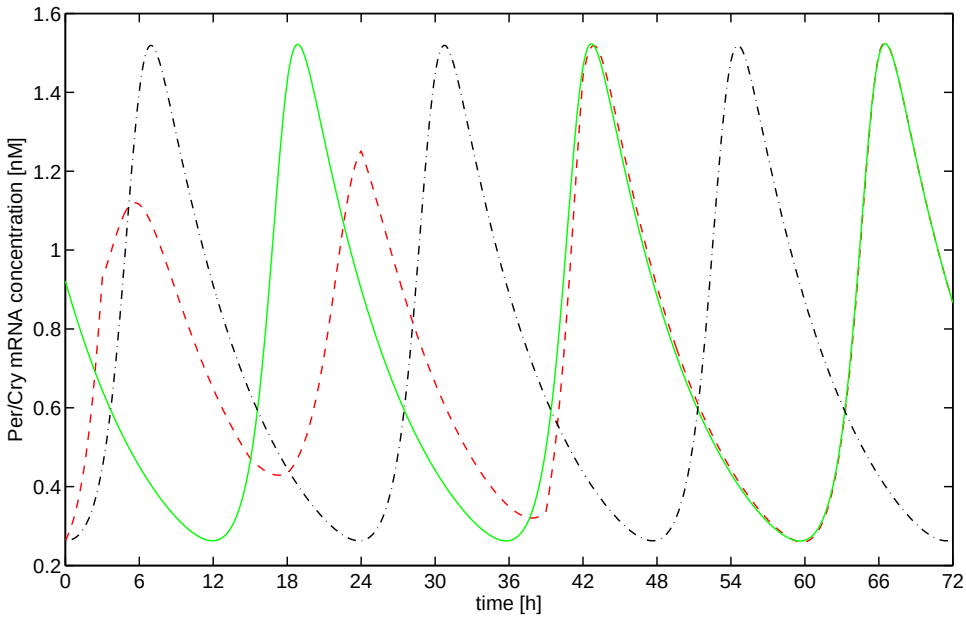

Fig. 5.5: Optimal control of circadian rhythm tracking of a 12-hour phase difference by light stimuli with multiple shooting. The solid curve represents the reference trajectory, the dashed curve shows the controlled system state trajectory (*Per2/Cry* mRNA concentration) and the dash-dot curve represents the uncontrolled system state trajectory (*Per2/Cry* mRNA concentration).

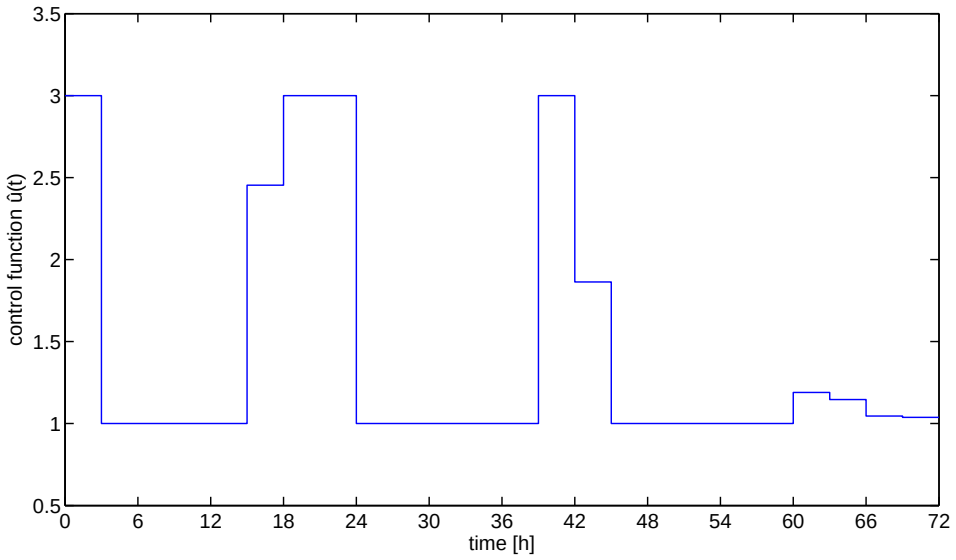

Fig. 5.6: Controls obtained by the numerical optimization with multiple shooting for a 12-hour phase shift. Values of the control function $\widehat{u}(t)$ are required to be in the interval $[1, 3]$.

Chapter 6
Conclusions

The goal of this thesis is to first give an integrated understanding of the mammalian circadian clock from the biological as well as the mathematical point of view in order to focus on the application of numerical optimal control theory to the mathematical clock model.

Organisms throughout species are influenced by daily and seasonal changes that result from the rotation of the Earth around the sun. This periodic pattern which is mainly displayed by the light-dark cycle has driven the development of endogenous circadian timing systems that synchronize biological functions to the environment. We first give a description of this biological system and explain the molecular mechanisms that generate the circadian rhythms.

This biological background knowledge is necessary in order to understand the construction and derivation of mathematical models representing the circadian clock that can contribute to a better understanding of the complex cellular processes.

The circadian clock can be modeled as a system of nonlinear ordinary differential equations. In chapter 3 we present a very simplified clock model which adequately represents the core of the circadian clock mechanism, a delayed negative feedback loop. We investigate the model with analytical methods and furthermore show how the generation of sustained oscillations depends on the way the reaction kinetics are modeled.

In the next chapter, a more detailed and realistic model of the mammalian circadian oscillator is introduced. After its derivation and numerical solution is explained, we include the modeling of light input and investigate the impact on the dynamic behavior of the system. All this preliminary knowledge serves as basis for the application of numerical control theory to the mammalian circadian clock model, which is done in chapter 5.

This chapter contains the major work of this thesis. One important feature of circadian oscillations is the phase response to light stimuli. The problem of phase tracking consists of shifting the system into a desired phase. After the necessary mathematical theory of optimal control and constrained nonlinear optimization is presented, we implement and solve the problem in MATLAB. In the numerical experiments it was possible to automatically identify optimal strength and timing of light stimuli that are able to recover a phase shift of up to 12 hours in less than three days.

The application of control theory to complex biological systems has become more and more important over the past few years and light therapy in general is certainly considered as a useful treatment for jet lag or the delayed sleep phase syndrome.

However, many further studies are necessary in order to obtain results that are actually feasible in a clinical setting. For example, controls representing continu-

ously adjustable light stimuli as shown in Figure 5.4 and Figure 5.6 are hard to realize in practice. For clinical treatment methods, be it light therapy or hormone administration, stimuli intensities will most likely be restricted to integer or even binary values. A powerful mixed-integer approach that allows to identify stimuli that switch between two given bounds for the control parameter has been presented in [30]. New insights could possibly be gained by the application of such an optimal control algorithm of mixed-integer type to a very detailed model of the mammalian circadian clock such as presented in [10].

Moreover, entrainment of the circadian oscillator in a more natural setting wherein light-dark cycles affect the response of the system during control has to be taken into account.

If further research is done, optimal control algorithms could provide great help in determining inputs that are able to optimally advance or delay the phase of the circadian oscillator or even to restore altered pathological rhythms thought to be present in many types of cancer [23].

Appendix A
Matlab implementations

A.1 Damped Newton's method

```
function x= Newton(x0,maxIt,tol,f,f2,a,b,c,p)
x = zeros(length(x0), maxIt);
d = zeros(length(x0), maxIt);
lambda = zeros(maxIt,1);
x(:,1)=x0;
lambda(1)=1;

for k =1:maxIt
y = f(x(:,k),a,b,c,p);
dy = f2(x(:,k),a,b,c,p);
d(:,k) = dy\y;
    if (norm(y)<tol)
    break;
    end
x(:,k+1)=x(:,k)-lambda(k)*d(:,k);
y = f(x(:,k+1),a,b,c,p);
while (norm(dy\y)>(1-lambda(k)/2)*norm(d(:,k)))
    lambda(k)=0.5*lambda(k);
    x(:,k+1)=x(:,k)-lambda(k)*d(:,k);
    y = f(x(:,k+1),a,b,c,m);
    if lambda(k)<0.001
        break;
    end
end
lambda(k+1)=min(1,2*lambda(k));
end

x=x(:,k);
end
```

A.2 Single shooting implementation

```
function singleshooting()
T=72;
d=36;
x0= [0.9214;1.4285;1.7455;1.3261;0.4912;0.6376;0.8887;
     0.2627;0.2795;1.1482;0.8280;0.6874;1.3419;1.0771;0];
q=ones(d,1);
lb=ones(length(q),1);
ub=3*ones(length(q),1);
options = optimset('Algorithm','active-set','Display','
   Iter','TolFun',1e-3, 'MaxFunEvals',1e6);
x =fmincon(@(q)disc(x0,q,T,d),q,[],[],[],[],lb,ub,[],
   options);

t=0:T/d:T;
figure
stairs(t',[x;x(end)])
xlabel('time [h]')
ylabel('control')

%objective function
function f = disc(x0,q,T,d)
t_help=[];
y_help=[];
[t,y] = ode45(@(t,y)system_for_optcontrol(t,y,q(1)),[0 T/d
   ],x0);
t_help=[t_help; t];
clear t;
y_help=[y_help; y];
clear y;
k=2;
for i=T/d : T/d : T-T/d
    [t,y] = ode45(@(t,y)system_for_optcontrol(t,y,q(k)),[i
       ,i+T/d],y_help(end,:));
    t_help=[t_help; t];
    clear t;
    y_help=[y_help; y];
    clear y;
    k=k+1;
end
f=y_help(end,15);
```

```
37
38 figure(1)
39 plot(t_help,y_help(:,8),'r--')
40 hold on
41 plot(t_help,y_help(:,1),'g')
42 hold off
43 xlabel('time [h]')
44 ylabel('Per2/Cry mRNA concentration [nM]')
45 clear y_help;
46 clear t_help;
```

A.3 Multiple shooting implementation

```
function multipleshooting()
T=72;
d=24;
x0= [0.9214;1.4285;1.7455;1.3261;0.4912;0.6376;0.8887;
     0.2627;0.2795;1.1482;0.8280;0.6874;1.3419;1.0771;0];
q=ones(d,1);

[t1,y0]=ode45(@model,0:T,x0(8:14));
s=[];
for i=T/d : T/d : T
s=[s;y0(i+1,:)'];
end

param=[q;s];
lb=[ones(length(q),1);zeros(length(s),1)];
ub=[3*ones(length(q),1);3*ones(length(s),1)];
options = optimset('Display','Iter', 'Algorithm','active-
   set','TolFun',1e-3, 'MaxFunEvals',1e6);

x =fmincon(@(param)disc(x0,param,T,d),param,[],[],[],[],lb
   ,ub,@(param)constraints(x0,param,T,d),options);
t=0:T/d:T;
figure(1)
stairs(t',[x(1:d);x(d)])
xlabel('time [h]')
ylabel('control')

%nonlinear contraints
function [c,ceq] = constraints(x0,param,T,d)
c=[];
t_help=[];
y_help=[];
[t,y] = ode45(@(t,y)system_for_optcontrol(t,y,param(1)),[0
    T/d],x0);
t_help=[t_help; t];
clear t;
y_help=[y_help; y];
yend= y(end,8:14)';
clear y;
k=2;
```

```
for i=T/d : T/d : T-T/d
    [t,y] = ode45(@(t,y)system_for_optcontrol(t,y,param(k)
       ),[i,i+T/d],[y_help(end,1:7)';param(d+1+(k-2)*7:d
       +1+(k-2)*7+6);y_help(end,15)]);
    t_help=[t_help; t];
    clear t;
    y_help=[y_help; y];
    yend = [yend; y(end,8:14)'];
    clear y;
    k=k+1;
end
ceq= yend-param(d+1:end);

%objective function
function f = disc(x0,param,T,d)
t_help=[];
y_help=[];
[t,y] = ode45(@(t,y)system_for_optcontrol(t,y,param(1)),[0
    T/d],x0);
t_help=[t_help; t];
clear t;
y_help=[y_help; y];
clear y;
k=2;
for i=T/d : T/d : T-T/d
    [t,y] = ode45(@(t,y)system_for_optcontrol(t,y,param(k)
       ),[i,i+T/d],[y_help(end,1:7)';param(d+1+(k-2)*7:d
       +1+(k-2)*7+6);y_help(end,15)]);
    t_help=[t_help; t];
    clear t;
    y_help=[y_help; y];
    clear y;
    k=k+1;
end
f=y_help(end,15);

figure(2)
plot(t_help,y_help(:,8),'r--')
hold on
plot(t_help,y_help(:,1),'g')
hold off
xlabel('time [h]')
```

```
75 ylabel('Per2/Cry mRNA concentration [nM]')
76 clear y_help;
77 clear t_help;
```

Bibliography

[1] A. Barclay, P. E. Gill and J. B. Rosen: SQP Methods and their Application to Numerical Optimal Control. Report NA 97−3, Dept of Mathematics, University of California, San Diego.

[2] S. Becker-Weimann: Modeling Feedback Loops in the Mammalian Circadian Oscillator. PhD thesis, Humboldt University of Berlin, 2008.

[3] H. G. Bock and K. J. Plitt: A multiple shooting algorithm for direct solution of optimal control problems. *Proceedings of the Ninth IFAC World Congress, Budapest*, Pergamon, Oxford, 1984.

[4] Y. Dagan: Circadian rhythm sleep disorders (CRSD). *Sleep Medicine Reviews (Elsevier)* 6(1):45−54, 2002.

[5] M. Diehl: Numerical Optimal Control. Optimization in Engineering Center (OPTEC) and Electrical Engineering Department (ESAT), K.U. Leuven, Belgium. `http://homes.esat.kuleuven.be/~mdiehl/TRONDHEIM/OptimalControl.pdf`.

[6] J. R. Dormand, and P. J. Prince: A family of embedded Runge-Kutta formulae. *J of Computational and Applied Mathematics*, 6 (1): 19−26, 1980.

[7] J. C. Dunlap: Molecular bases for circadian clocks. *Cell*, 96(2):271−90, 1999.

[8] J. C. Dunlap: Chronobiology - Biological Timekeeping. Sinauer Associates, Inc., Sunderland, 2004.

[9] C. Fall, E. Marland, J. Wagner and J. Tyson: Computational Cell Biology. Springer, 2002.

[10] D. Forger and C. Peskin: A detailed predictive model of the mammalian circadian clock. *Proc Natl Acad Sci U S A*, 100(25):14806−11, 2003.

[11] N. Gekakis, D. Staknis, H. B. Nguyen, F. C. Davis, L. D. Wilsbacher, D. P. King, J. S. Takahashi, and C. J. Weitz: Role of the CLOCK protein in the mammalian circadian mechanism. *Science*, 280(5369):1564−1569, 1998.

[12] L. Glass and M. C. Mackey: From Clocks to Chaos: The Rhythms of Life. Princeton University Press, 1988.

[13] B. C. Goodwin: Oscillatory behavior in enzymatic control processes. *Adv Enzyme Regul*, 3:425−439, 1965.

[14] A. Griewank: Evaluating Derivatives: Principles and Techniques of Algorithmic Differentiation. *Frontiers in Appl. Math.*, SIAM, 2000.

[15] J. Griffith: Mathematics of cellular control processes. I. Negative feedback to one gene. *J Theor Biol*, 20(2):202−8, 1968.

[16] J. C. Hall and M. Rosbash: Genes and biological rhythms. *Trends in Genetics*, 3:185−191, 1987.

[17] G. Hardy, J. Littlewood, and G. Poyla: Inequalities. Cambridge University Press, Cambridge, UK, 1988.

[18] D. Lebiedz: Skript zur Vorlesung Optimierung I, Universität Freiburg, 2011.

[19] J. Leloup and A. Goldbeter: Toward a detailed computational model for them mammalian circadian clock. *Proc Natl Acad Sci U S A*, 100(12):7051−6, 2003.

[20] R. Manfredini, F. Manfredini, C. Fersini and F. Conconi: Circadian rhythms, athletic performance, and jet lag. *Br J Sports Med*, 32:101−106, 1998.

[21] E. Maywood, J. OBrien, and M. Hastings: Expression of mCLOCK and other circadian clock-relevant proteins in the mouse suprachiasmatic nuclei. *J Neuroendocrinol*, 15(4):329−34, 2003.

[22] S. Miyake, Y. Sumi, L. Yan, S. Takekida, T. Fukuyama, Y. Ishida, S. Yamaguchi, K. Yagita, and H. Okamura: Phase-dependent responses of Per1 and Per2 genes to a light-stimulus in the suprachiasmatic nucleus of the rat. *Neurosci Lett*, 294(1):41−4, 2000.

[23] M. C. Mormont, J. Waterhouse, P. Bleuzen, S. Giachetti, A. Jami, A. Bogdan, J. Lellouch, J. L. Misset, Y. Touitou and F. Levi: Marked 24 h rest/activity rhythms are associated with better quality of life, better response, and longer survival in patients with metastatic colorectal cancer and good performance status. *Clin. Cancer Res.*, 6, pp. 3038−3045, 2000.

[24] N. Preitner, F. Damiola, L. Lopez-Molina, J. Zakany, D. Duboule, U. Albrecht, and U. Schibler: The orphan nuclear receptor REV-ERBα controls circadian transcription within the positive limb of the mammalian circadian oscillator. *Cell*, 110(2):251−260, 2002.

[25] S. M. Rajaratnam and J. Arendt: Health in a 24-h society. *Lancet*, 358, pp. 999−1005, 2001.

[26] M. S. Rea, A. Bierman, M.G. Figueiro, and J.D. Bullough: A new approach to understanding the impact of circadian disruption on human health. *Journal of Circadian Rhythm*, 6, 2008.

[27] Q. R. Regestein and M. Pavlova: Treatment of Delayed Sleep Phase Syndrome. *General Hospital Psychiatry*, 17, 335−345, 1995.

[28] M. Rehberg and D. Lebiedz: Phase tracking of circadian rhythm by model-based optimal control. Proceedings of the Third International Conference on Foundations of Systems Biology in Engineering, Denver, CO, USA, 2009.

[29] S. M. Reppert and D. R. Weaver: Coordination of circadian timing in mammals. *Nature*, 418(6901):935−941, 2002.

[30] O.S. Shaik, S. Sager, O. Slaby, and D. Lebiedz: Phase tracking and restoration of circadian rhythms by model-based optimal control. *IET Syst Biol*, Vol. 2, No. 1, 2008.

[31] S. H. Strogatz: Nonlinear dynamics and chaos. Perseus Books Publishing, LLC, Cambridge, 1994.

[32] M. J. Zylka, L. P. Shearman, D. R. Weaver and S. M. Reppert: Three period Homologs in Mammals: Differential Light Responses in the Suprachiasmatic Circadian Clock and Oscillating Transcripts Outside of Brain. *Neuron*, Vol. 20, 1103−1110, 1998.

Ehrenwörtliche Erklärung

Ich erkläre hiermit ehrenwörtlich, dass ich die vorliegende Arbeit selbstständig angefertigt habe; die aus fremden Quellen direkt oder indirekt übernommenen Gedanken sind als solche kenntlich gemacht. Die Arbeit wurde bisher keiner anderen Prüfungsbehörde vorgelegt und auch noch nicht veröffentlicht.

Ich bin mir bewusst, dass eine unwahre Erklärung rechtliche Folgen haben wird.

Ulm, den 14. September 2012 _____

(Unterschrift)